International Journal on Future Revolution in Computer Science & Communication Engineering
Volume: 4 Issue: 2
ISSN: 2454-4248
378 – 387

Image Enhancement by Elliptic Discrete Fourier Transforms

Artyom M. Grigoryan
Department of Electrical and Computer Engineering
University of Texas at San Antonio
San Antonio, TX 78249-0669
amgrigoryan@utsa.edu

Sos S. Agaian
Computer Science Department
The College of Staten Island
New York, USA
Sos.Agaian@csi.cuny.edu

***Abstract*—**This paper describes a method of enhancement of grayscale and color image in the frequency domain by the pair of two elliptic discrete Fourier transforms (EDFT). Unlike the traditional discrete Fourier transform (DFT), the EDFT is parameterized and the parameter defines ellipses (not circles) around which the input data are rotated. Methods of the traditional DFT are widely used in image enhancement, and the transform rotates data of images around the circles. The presented method of image enhancement proposes processing images on different set of ellipses for the direct and inverse transforms. Our preliminary experimental examples show effectiveness of the proposed method. The Illustrative examples of image enhancement are given.

Keywords *- Image enhancement,discrete Fourier transform, elliptic discrete Fourier transform, measure of enhancement.*

*****

I. INTRODUCTION

Transform-based image enhancement is one of the main classes of methods in enhancement [1]-[10], which is effective and simple in implementation because of using fast transforms [14]-[21]. The main transform in this class is the discrete Fourier transform (DFT), which allows not only for enhancement but filtration of images as well. As an example, we mention the known alpha-rooting method of image enhancement, when the only magnitude of the 2-D DFT of the image is changed, living the phase the same at each frequency-points [11]-[13]. The phase is a very sensitive characteristic of the transform and the small changes in the phase may cause the big changes in images. Another method of image enhancement is the retinex algorithm, which uses the fast methods of the 2-D DFT for convoluting the image with Gaussian filters with different scales [27]. Methods of color image enhancement by the quaternion 2-D DFTs are also effectively used [28]-[30].

In this paper, we describe a simple method of image enhancement, by using the concept of the elliptic DFT. Considering the geometry of the traditional DFT, we can state that this transform rotates data around the circles, and manipulation with its coefficients can be described by a process of moving rotated points from circles to other circles. Then, the inverse DFT is rotated the obtained points on the new circles in opposite direction, namely clockwise. The parameter of the elliptic DFT defines the ellipses around which the data are rotated. Only using the direct and inverse EDFT with different values of this parameter changes the original image. In other words, it is the simplest image processing procedure in the frequency domain. The goal of our work is to show that the pair of the direct and inverse EDFT with different parameters may lead to effective enhancement of grayscale and color images.

II. DFT IN MATRIX FORM

Given a real or complex signal f_n of length N, we consider the N-point DFT defined as

$$F_p = \sum_{n=0}^{N-1} f_n W(n,p) = \sum_{n=0}^{N-1} f_n W^{np}, \qquad (1)$$

for $p = 0:(N-1)$.

Here, the exponential kernel of the transform is defined as the set of N equidistant points on the unit circle

$$W^{np} = W_N^{np} = e^{-i\frac{2\pi}{N}np} = \cos\left(\frac{2\pi}{N}np\right) - i\sin\left(\frac{2\pi}{N}np\right).$$

The matrix of the N-point DFT is

$$[F] = \begin{bmatrix} 1 & 1 & 1 & 1 & \vdots & 1 \\ 1 & W^1 & W^2 & W^3 & \vdots & W^{N-1} \\ 1 & W^2 & W^4 & W^6 & \vdots & W^{N-2} \\ 1 & \vdots & \vdots & \vdots & \vdots & \vdots \\ 1 & W^{N-2} & W^{N-4} & W^{N-6} & \vdots & W^2 \\ 1 & W^{N-1} & W^{N-2} & W^{N-3} & \vdots & W^1 \end{bmatrix}.$$

Each product $f_n W^{np}$ in the sum of (1) represents the rotation, if we consider the complex number $f_n = x_n + iy_n$ as a point (x_n, y_n) in the two-dimension plane. Indeed, let $k = np$, and let $c_k = \cos(2\pi k/N)$ and $s_k = \sin(2\pi k/N)$, then

$$f_n W^k = (x_n + iy_n)(c_k - is_k) = (c_k x_n + s_k y_n) + i(-s_k x_n + cy_n).$$

If we denote the real and imaginary part of $f_n W^k$ by A and B, then in matrix form this product can be written as

$$f_n W^k = (A,B) \to \begin{pmatrix} A \\ B \end{pmatrix} = \begin{pmatrix} c_k x_n + s_k y_n \\ -s_k x_n + cy_n \end{pmatrix} = T^k \begin{pmatrix} x_n \\ y_n \end{pmatrix}.$$

where the matrix

$$T^k = \begin{pmatrix} c_k & s_k \\ -s_k & c_k \end{pmatrix} = \begin{pmatrix} \cos(\varphi_k) & \sin(\varphi_k) \\ -\sin(\varphi_k) & \cos(\varphi_k) \end{pmatrix}. \qquad (2)$$

This matrix is the matrix of elementary rotation, or the Givens rotation by the angle $\varphi_k = 2\pi k/N$. Therefore denoting by R_p and I_p the real and imaginary parts of F_p, the N-point DFT at the frequency-point p can be written as

 ISSN: 2454-4248
378 – 387

$$F_p = (R_p, I_p) \to \begin{pmatrix} R_p \\ I_p \end{pmatrix} = \sum_{n=0}^{N-1} T^{np} \begin{pmatrix} x_n \\ y_n \end{pmatrix}. \qquad (3)$$

Considering the signal and its DFT as the column-vectors

$$\boldsymbol{f} = (f_0, f_1, \dots, f_{N-1})' = (x_0, y_0, x_1, y_1, \dots, x_{N-1}, y_{N-1})'$$

and

$$\boldsymbol{F} = (F_0, F_1, \dots, F_{N-1})' = (R_0, I_0, R_1, I_1, \dots, R_{N-1}, I_{N-1})',$$

we can write the N-point DFT in the following matrix form

$$\begin{bmatrix} R_0 \\ I_0 \\ R_1 \\ I_1 \\ \vdots \\ R_{N-1} \\ I_{N-1} \end{bmatrix} = \begin{bmatrix} I & I & I & I & \dots & I & I \\ I & T^1 & T^2 & T^3 & \dots & T^{N-2} & T^{N-1} \\ I & T^2 & T^4 & T^6 & \dots & T^{N-4} & T^{N-2} \\ I & T^3 & T^6 & T^9 & \dots & T^{N-6} & T^{N-3} \\ \vdots & \vdots & \vdots & \vdots & \dots & \vdots & \vdots \\ I & T^{N-2} & T^{N-4} & T^{N-6} & \dots & T^4 & T^2 \\ I & T^{N-1} & T^{N-2} & T^{N-3} & \dots & T^2 & T^1 \end{bmatrix} \begin{bmatrix} x_0 \\ y_0 \\ x_1 \\ y_1 \\ \vdots \\ x_{N-1} \\ y_{N-1} \end{bmatrix}.$$

In this equation, the DFT in the real space R^{2N} is described by the matrix

$$\boldsymbol{T} = \begin{bmatrix} I & I & I & I & \dots & I & I \\ I & T^1 & T^2 & T^3 & \dots & T^{N-2} & T^{N-1} \\ I & T^2 & T^4 & T^6 & \dots & T^{N-4} & T^{N-2} \\ I & T^3 & T^6 & T^9 & \dots & T^{N-6} & T^{N-3} \\ \vdots & \vdots & \vdots & \vdots & \dots & \vdots & \vdots \\ I & T^{N-2} & T^{N-4} & T^{N-6} & \dots & T^4 & T^2 \\ I & T^{N-1} & T^{N-2} & T^{N-3} & \dots & T^2 & T^1 \end{bmatrix} \qquad (4)$$

which is the $N \times N$ block-matrix, each block of which is the 2×2 matrix of the Givens rotation. The matrix $I = I_2$ is the 2×2 identity matrix. The 2×2 matrices of rotation are periodic,

$$T^0 = T^N = I, \qquad T^k = T^{k+N} = T^{k-N},$$

for $k = 0{:}(N-1)$, and it is not difficult to see that $T^{k_1+k_2} = T^{k_1}T^{k_2}$, for any two integers k_1 and k_2.

Thus, in the N-point DFT lies the idea of clock-wise rotating each value, or point of the input data $f_n = x_n + iy_n = (x_n, y_n)$ around the circle of radius $r_n = \sqrt{x_n^2 + y_n^2}$ by the corresponding angle $\varphi_{np} = (2\pi/N)np = np\varphi_1$. The first value $f_0 = x_0 + iy_0 = (x_0, y_0)$ is not rotated; $\varphi_0 = 0$. After rotating all input points, the rotated points are projected on the X-axis and added together and then projected on the Y-axes and added, too. These sums represent the real and imaginary values of the component F_p. It should be noted that, for the $p = 0$ case, all angles $\varphi_{n0} = 0$ and the calculation of the first component F_0 is reduced to summing separately the coordinates of the input points (x_n, y_n), $n = 0{:}(N-1)$.

III. DFT WITH ROTATIONS AROUND ELLIPSES

In this section, we consider the transform with the $N \times N$ block-matrix that is similar to the matrix $\boldsymbol{T}$ for the N-point DFT, but which is composed not by matrices of the Givens rotations. We consider the rotations around ellipses.

Instead of the Givens rotations, the Grigoryan rotations are considered, which are also the Nth roots of the 2×2 identity matrix I [22]-[24]. The matrices of such rotations are defined in the following way. Given the angle $\varphi = \varphi_1 = 2\pi/N$, let $E(\varphi)$ be the matrix

$$G = G(\varphi) = \begin{bmatrix} \cos(\varphi) & \cos(\varphi) - 1 \\ \cos(\varphi) + 1 & \cos(\varphi) \end{bmatrix}. \qquad (5)$$

It is not difficult to see that $\det(G) = 1$ the matrix E can be written as

$$G = \cos(\varphi)\, U + V = \cos(\varphi) \begin{bmatrix} 1 & 1 \\ 1 & 1 \end{bmatrix} + \begin{bmatrix} 0 & -1 \\ 1 & 0 \end{bmatrix}.$$

Here, the matrices

$$U = \begin{bmatrix} 1 & 1 \\ 1 & 1 \end{bmatrix} \text{ and } V = \begin{bmatrix} 0 & -1 \\ 1 & 0 \end{bmatrix}.$$

We also can consider the representation that is similar to the exponent $\exp(i\varphi) = \cos(\varphi) + \sin(\varphi)i$, namely,

$$G = \cos(\varphi)\, I + \sin(\varphi)\, R, \qquad (6)$$

where the parameterized matrix

$$R = R(\varphi) = \begin{bmatrix} 0 & -\tan(\varphi/2) \\ \cot(\varphi/2) & 0 \end{bmatrix}. \qquad (7)$$

The determinant of this matrix is 1, $\det R(\varphi) = 1$, and its square is

$$R^2(\varphi) = -I. \qquad (8)$$

It is not difficult to see that $G^N(\varphi) = I$ for any integer N.

Example 1: For the $N = 9$ case, the angle $= 2\pi/9$, $\cos(\varphi) = 0.7660$, and the matrix

$$G = \cos(\varphi) \begin{bmatrix} 1 & 1 \\ 1 & 1 \end{bmatrix} + \begin{bmatrix} 0 & -1 \\ 1 & 0 \end{bmatrix} = \begin{bmatrix} 0.7660 & -0.2340 \\ 1.7600 & 0.7660 \end{bmatrix}.$$

We also have the following:

$$R = \begin{bmatrix} 0 & -\tan(\varphi/2) \\ \cot(\varphi/2) & 0 \end{bmatrix} = \begin{bmatrix} 0 & -0.3640 \\ 2.7475 & 0 \end{bmatrix},$$

$\det R = 1$, and

$$G = 0.7660\, I + 0.6428 R = \begin{bmatrix} 0.7660 & -0.2340 \\ 1.7600 & 0.7660 \end{bmatrix}.$$

The next eight powers of this matrix are

$$G^2 = \begin{bmatrix} 0.1736 & -0.3584 \\ 2.7057 & 0.1736 \end{bmatrix}, G^3 = \begin{bmatrix} -0.5 & -0.3152 \\ 2.3794 & -0.5 \end{bmatrix},$$
$$G^4 = \begin{bmatrix} -0.9397 & -0.1245 \\ 0.9397 & -0.9397 \end{bmatrix}, G^5 = \begin{bmatrix} -0.9397 & 0.1245 \\ -0.9397 & -0.9397 \end{bmatrix},$$
$$G^6 = \begin{bmatrix} -0.5 & 0.3152 \\ -2.3794 & -0.5 \end{bmatrix}, G^7 = \begin{bmatrix} 0.1736 & 0.3584 \\ -2.7057 & 0.1736 \end{bmatrix},$$
$$G^8 = \begin{bmatrix} 0.7660 & 0.2340 \\ -1.7600 & 0.7660 \end{bmatrix}, G^9 = \begin{bmatrix} 1 & 0 \\ 0 & 1 \end{bmatrix}.$$

 ISSN: 2454-4248
378 – 387

The list of these nine matrices includes their inverse matrices as well. Indeed,

$$G^{-1} = G^8, G^{-2} = G^7, G^{-3} = G^6, G^{-4} = G^5. \quad (9)$$

This property can be written as $G^{-k} = G^{9-k}$, for $k = 1{:}8$.

Now, we consider the following 9×9 block matrix

$$\boldsymbol{M}(G) = \begin{bmatrix} I & I & I & I & I & I & I & I & I \\ I & G^1 & G^2 & G^3 & G^4 & G^5 & G^6 & G^7 & G^8 \\ I & G^2 & G^4 & G^6 & G^8 & G^1 & G^3 & G^5 & G^7 \\ I & G^3 & G^6 & I & G^3 & G^6 & I & G^3 & G^6 \\ I & G^4 & G^8 & G^3 & G^7 & G^2 & G^6 & G^1 & G^5 \\ I & G^5 & G^1 & G^6 & G^2 & G^7 & G^3 & G^8 & G^4 \\ I & G^6 & G^3 & I & G^6 & G^3 & I & G^6 & G^3 \\ I & G^7 & G^5 & G^3 & G^1 & G^8 & G^6 & G^4 & C^2 \\ I & G^8 & G^7 & G^6 & G^5 & G^4 & G^3 & G^2 & G^1 \end{bmatrix}.$$

Considering the numbering by $n = 0{:}8$ along the rows and by $p = 0{:}8$ along the columns, the (n, m)-th block in this matrix is the 2×2 matrix $G^{np} = G^{np \bmod 9}$. This matrix is symmetric, since $G^{np} = G^{pn}$.

The determinant of this matrix is $387420489 = 9^9$ and the 4th power $\boldsymbol{M}^4(G) = 81I_{18}$. The same properties hold for the 9-point DFT. Indeed, if we construct the 9×9 block matrix $\boldsymbol{M}(T)$, by using the Givens rotation $T = T(\varphi)$, then the determinant of this matrix will also be 9^9 and $\boldsymbol{M}^4(T) = 81I_{18}$.

It is important to note that, if we compose the similar 9×9 block matrix with the basic matrix G^{-1}, i.e., (G^{-1}), then we obtain the following equality:

$$\boldsymbol{M}(G)\boldsymbol{M}(G^{-1}) = 9\boldsymbol{E}.$$

Here $\boldsymbol{E}$ is the 18×18 identity matrix. Thus, the inverse matrix is

$$\boldsymbol{M}^{-1}(G) = \frac{1}{9}\boldsymbol{M}(G^{-1}), \quad (10)$$

and using Eq. (9), we obtain

$$\boldsymbol{M}^{-1}(G) = \frac{1}{9}\begin{bmatrix} I & I & I & I & I & I & I & I & I \\ I & G^8 & G^7 & G^6 & G^5 & G^4 & G^3 & G^2 & G^1 \\ I & G^7 & G^5 & G^3 & G^1 & G^8 & G^6 & G^4 & G^2 \\ I & G^6 & G^3 & I & G^6 & G^3 & I & G^6 & G^3 \\ I & G^5 & G^1 & G^6 & G^2 & G^7 & G^3 & G^8 & G^4 \\ I & G^4 & G^8 & G^3 & G^7 & G^2 & G^6 & G^1 & G^5 \\ I & G^3 & G^6 & I & G^3 & G^6 & I & G^3 & G^6 \\ I & G^2 & G^4 & G^6 & G^8 & G^1 & G^3 & G^5 & G^7 \\ I & G^1 & G^2 & G^3 & G^4 & G^5 & G^6 & G^7 & G^8 \end{bmatrix}.$$

The transform with the 9×9 block matrix $\boldsymbol{M}(G)$ is called the G-matrix generalized discrete transform (G-GDT). This transform is also called the 9-point elliptical discrete Fourier transform (EDFT), because during the transformations

$$z \to Gz \to G^2z \to G^3z \to G^4z \to \cdots \to G^8z \to G^9z = z$$

the point $z = (x_0, y_0) = (1{,}0)$ moves around the ellipse that is described by the equation

$$x^2 + \frac{y^2}{b^2} = 1, \quad (11)$$

where the semi-minor axis $b = \cot(\varphi/2) = 2.7475$. When using the matrix T instead of G, the point z moves around the unit circle $x^2 + y^2 = 1$.

In the general case of integer $N > 1$, the $N \times N$ block matrix $M(G)$ composed by the basic 2×2 matrix G given in Eq. (7) defines the N-point discrete transform that is called *the elliptic discrete Fourier transformation of type I*, or simply N-point EDFT [24]. This transform has the following properties:

$$\begin{aligned} \det \boldsymbol{M}(G) &= N^N, \\ \boldsymbol{M}^4(G) &= N^2 1I_{2N}, \\ \boldsymbol{M}^{-1}(G) &= \boldsymbol{M}(G^{-1})/N. \end{aligned} \quad (12)$$

The ellipse of rotation the point (1,0) is the same as in Eq. (10), with $b = \cot(\varphi/2)$, where the angle $\varphi = 2\pi/N$. The point (1,0) is the first point on the unit circle. Therefore, the geometry of the EDFT will be described by the ellipse in Eq. 11. Other points (x_0, y_0) are moving around similar ellipses.

IV. Difference between EDFT and DFT

It should be noted that when the matrix is

$$R(\phi) = \begin{bmatrix} 0 & 1 \\ -1 & 0 \end{bmatrix},$$

the matrix $G(\varphi, \phi)$ is the matrix of the Givens rotation. This is the case, when $\tan(\phi/2) = -1$, or $\phi = 7\pi/2$. If we consider the $\phi = \varphi$ case, then from the condition $\varphi = 2\pi/N = 7\pi/2$, we obtain that N should not be integer, but 4/7. We can obtain the rotation counter clock-wise around the circle for the $\phi = \varphi$ case, when $\tan(\varphi/2) = 1$, i.e., $\pi/N = \pi/4$; this is the $N = 4$ case.

The semi-minor axis $b = \cot(\varphi/2)$ grows up fast with large values of N. Indeed, for the values of $N = 4{:}10$, the values of b equal 1, 1.3764, 1.7321, 2.0765, 2.4142, 2.7475, 3.0777, respectively. As an example, we consider the rotation of integer numbers, when the 128-point EDFT is used. The geometry of this transform is described by the ellipse which is shown in Fig. 1. This ellipse has the semi-minor axis equal 40.7355 and it is the orbit of the point (1,0). The unit circle for this point when using the traditional 128-point DFT is also shown for comparison.

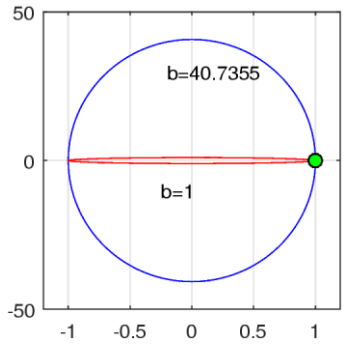

Figure 1. The elliptic orbit of the point (1,0) for the 128-point EDFT.

 ISSN: 2454-4248
378 – 387

This example shows how much different the concepts of the N-point DFT and EDFT. The orbit of the movement of a point, which is ellipse, changes with the order N of the EDFT. Rotation of each point $z = (x, y)$ during calculation of the classical N-point DFT is accomplished around the same circle of radius $|z|$. Because of the large semi-minor $b \gg 1$, the changes in calculation of the EDFT occur much along the vertical. It means that the imaginary part of the EDFT can be much enhanced in comparison with the N-point DFT.

Also, it is important to note that in the definition of the basic transform C in Eq. (6), we can consider other matrices R, for instance the matrices that are defined by angles $\phi \neq \varphi$,

$$R(\phi) = \begin{bmatrix} 0 & -\tan(\phi/2) \\ \cot(\phi/2) & 0 \end{bmatrix}. \qquad (12)$$

Indeed, $\det R(\phi) = 1$, $R^2(\phi) = -I$, and the parameterized matrix G can be defined as

$$G = G(\varphi, \phi) = \cos(\varphi)\, I + \sin(\varphi)\, R(\phi) \qquad (13)$$

or

$$G = \begin{bmatrix} \cos(\varphi) & -\sin(\varphi)\tan(\phi/2) \\ \sin(\varphi)\cot(\phi/2) & \cos(\varphi) \end{bmatrix}.$$

In this general case, we have the equality $G^N(\varphi, \phi) = I$, for any integer $N > 1$. The same ellipse given in Eq. (10) with the semi-minor $b = \cot(\phi/2)$ is the locus of all rotated points $G^n z$, when $n = 0{:}N-1$.

To show the changes, when applying the basic matrix $G(\varphi, \phi)$ in the N-point EDFT for the angle $\phi \neq \varphi$, we consider the $N = 9$ case and the movement of the point $z = (1,0)$ under the transformations G^k, when $k = 2{:}8$. Figure 2(a) shows one orbit of the point z in the $\phi = \varphi = 2\pi/9$ case and another orbit when $\phi = \varphi + \pi/9$. The addition angle $+\pi/9$ shrinks the orbit inside the first orbit. The case when $\phi = \varphi - \pi/9$ is shown in part (b). The point z moves along the greater orbit than the orbit of z when $\phi = \varphi$.

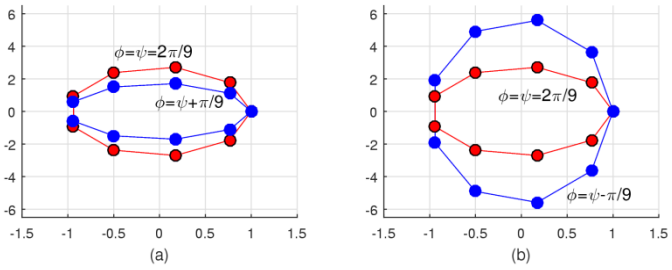

Figure 2. The orbits of the point (1,0) when (a) $\phi = 2\pi/9$ and $3\pi/9$ and (a) $\phi = 2\pi/9$ and $\pi/9$.

The orbits of other points may intersect as well. As an example, Figure 3 shows two orbits of the point $z = (x_0, y_0) = (1,2)$ in the $\phi = \varphi = 2\pi/9$ and $\phi = \varphi + \pi/9$ cases. This point is rotated around the ellipse that is described by

$$x^2 + \frac{y^2}{b^2} = r^2, \qquad b = \cot(\phi/2), \qquad (14)$$

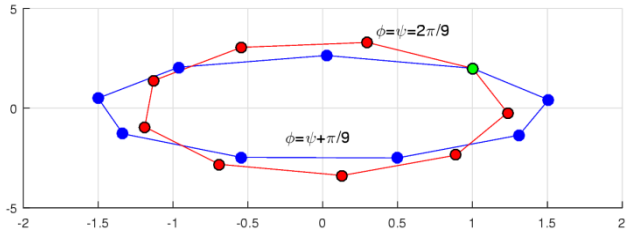

Figure 3. The orbits of the point (1,2) when $\phi = 2\pi/9$ and $3\pi/9$.

where the value of r^2 is calculated by

$$r^2 = {x_0}^2 + \frac{{y_0}^2}{b^2} = 1 + \frac{4}{b^2}.$$

When $\phi = \varphi = 2\pi/9$, then $b^2 = 3$ and $r^2 = 5/3 = 1.6667$. In the $\phi = 3\pi/9$ case, $b^2 = 7.5486$ and $r^2 = 1.5299$.

V. Method of Image Enhancing by EDFT

In this section, we apply the concept of the EDFT for image enhancement. The application is based on the reasoning given in Section IV. In the general definition of the N-point EDFT with the additional angle ϕ, i.e., when using the basic matrix $G(\varphi, \phi)$, this additional angle ϕ allows for changing the orbits of movements of points for the same value of N.

The 2-D EDFT of the image of size $N \times M$ is defined as the separable transform, which means that 1-D M-point EDFTs are calculating first over each row of the image and, then, 1-D N-point EDFTs are calculated by columns of the obtained matrix/data. In matrix form this transform can be written as

$$\boldsymbol{M}_{N,M}(G)\boldsymbol{f} = P_2 \boldsymbol{M}_N(G) P_1 [\boldsymbol{f} \boldsymbol{M}_M(G)^T]. \qquad (15)$$

Here, $\boldsymbol{M}_N(G)$ and $\boldsymbol{M}_M(G)$ denote the block matrices $\boldsymbol{M}(G)$ of the N- and M-point EDFTs, respectively. The matrix $\boldsymbol{M}_M(G)$ is of size $2M \times 2M$ and the image with its components $f_{n,m} = (r_{n,m}, i_{n,m})$ is written as the $N \times 2M$ matrix $\boldsymbol{f}$. After processing by rows, the obtained $N \times 2M$ data are written by the operator of permutation P_1 in form of $2N \times M$ matrix; each pair in rows of obtained elements is written as a column. Then, the $2N \times 2N$ matrix of the N-point EDFT is applied to each column of the permuted matrix. The result is the $2N \times M$ matrix that is permuted to the $N \times 2M$ matrix by permutation P_2. Here, each two numbers in columns sequentially are recorded as two numbers in rows.

For the N-point EDFT, the angle φ of the basic matrix $G(\varphi, \phi)$ is calculated uniquely as $\varphi = 2\pi/N$. Therefore, we can write briefly $G(\varphi, \phi)$ as $G(\phi)$. In the definition of the 2-D EDFT that is given in Eq. 15, it is assumed that the same second angle ϕ is used for both N- and M-point EDFTs.

Now, we consider the following method of image processing $\boldsymbol{f} \to \hat{\boldsymbol{f}}$ in the frequency domain:

$$\boldsymbol{f} \to \boldsymbol{g} = \boldsymbol{M}_{N,M}\big(G(\phi_1)\big)\boldsymbol{f} \to \hat{\boldsymbol{f}} = \boldsymbol{M}_{N,M}(G^{-1}(\phi_2))\boldsymbol{g}, \quad (16)$$

where ϕ_1 and ϕ_2 are two given angles. If these angles are equal, then the result of processing is $\hat{\boldsymbol{f}} = \boldsymbol{f}$. If the angles are different, the inverse 2-D EDFT changes the orbits when rotating back the data of the first 2-D EDFT of the image $\boldsymbol{f}$.

 ISSN: 2454-4248
378 – 387

When we applying the concept of the EDFT to signals, the transform increases much the amplitude of the imaginary part and leaves the real part of the rotated point in the same range. For the integer-valued input, it is not difficult to analyze the rotation of integer points. The integer points $(x, 0)$ are rotated by similar ellipses with large values of semi-minor axes. Figure 4 shows the ellipses around which the points (1,0), (2,0), (3,0), (4,0), and (5,0) are rotated, for the $\phi = \varphi = 2\pi/128$ case.

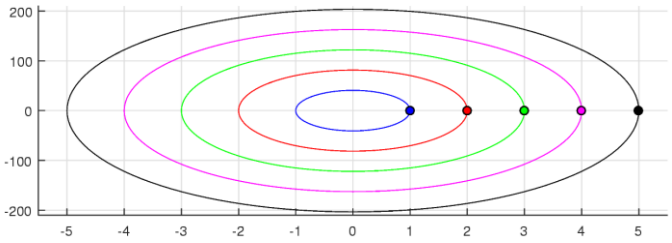

Figure 4. The orbits of five points $(x, 0), x = 1{:}\,5$, for the 128-point EDFT.

When the second angle $\phi > \varphi = 2\pi/N = \pi/64$, the semi-minor axis as the function $b = \cot(\phi/2)$ decreases, which mean that the rotation of the data presenting the direct 2-D EDFT will be moved from all orbits to lover orbits and it changes values of the transform. Thus, this parameter ϕ controls the sizes of orbits of rotations in the process of calculation of the EDFT. As an example, Fig. 5 shows new orbits (or ellipses) of the same five points $(x, 0)$, when the second angle is changed a little as $\phi = \varphi + 0.05$, i.e., plus about 3°.

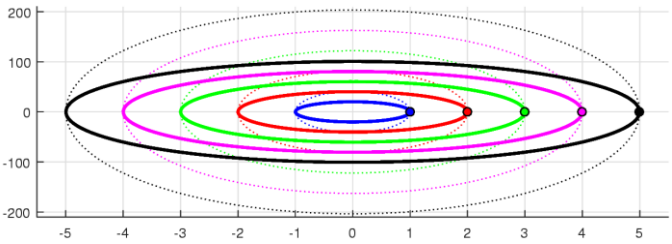

Figure 5. The orbits of five points $(x, 0), x = 1{:}\,5$, for the 128-point EDFT with $\phi = \varphi + 0.05 = \pi/64 + 0.05$.

Now, we consider the special case when $G = G(\varphi)$, i.e., $\phi = \varphi = 2\pi/N$, and input data for the elliptical DFT are real. When applying the N-point EDFT on the real data, the transform differs from the traditional DFT in the imaginary part; the real parts are the same. Indeed, the Givens rotations by the angle $n\varphi = 2\pi n/N$ are described by matrices

$$T^{n\varphi} = \begin{bmatrix} \cos(n\varphi) & \sin(n\varphi) \\ -\sin(n\varphi) & \cos(n\varphi) \end{bmatrix}.$$

Therefore, the real vector $(x, 0)$ is rotated as

$$T^{n\varphi} \begin{pmatrix} x \\ 0 \end{pmatrix} = \begin{pmatrix} x\cos(n\varphi) \\ -x\sin(n\varphi) \end{pmatrix}.$$

It is not difficult to verify, that the same coefficients $\cos(n\varphi)$ lies on the main diagonal of the matrix

$$G^{np} = \begin{bmatrix} \cos(\varphi) & -\sin(\varphi)\tan(\phi/2) \\ \sin(\varphi)\cot(\phi/2) & \cos(\varphi) \end{bmatrix}^{np}.$$

For instance,

$$G^{2} = \begin{bmatrix} \cos(2\varphi) & -\sin(2\varphi)\tan(\phi/2) \\ \sin(2\varphi)\cot(\phi/2) & \cos(2\varphi) \end{bmatrix}.$$

The application of this matrix on the real vector $(x, 0)$ is

$$G^{2} \begin{pmatrix} x \\ 0 \end{pmatrix} = \begin{pmatrix} x\cos(2\varphi) \\ x\sin(2\varphi)\cot(\phi/2) \end{pmatrix},$$

and $\cot(\phi/2) > 1$ for small angles, like $\phi = \varphi = 2\pi/N$, when $N > 8$. Therefore, the N-point EDFT changes the component of the DFT (R_p, I_p) at the frequency-point p as

$$(R_p, I_p) \to \left(R_p, -I_{N-p}\cot(\phi/2)\right), \qquad (17)$$

where $p = 1{:}\,(N-1)$.

As an example, we consider the $N = 36$ case with the discrete signal

$$x(t) = 5 + 0.1\cos(2\omega_0 t) + 0.2\cos(5\omega_0 t) + 4\sin(6\omega_0 t)$$

that is sampled in the time-interval $[0, 2\pi]$. Here, the frequency $\omega_0 = 0.4$. Figure 6 shows the discrete signal $x(n)$ in part (a) and the real part of the 36-point EDFT is part (b). The transform is cyclically shifted to the center.

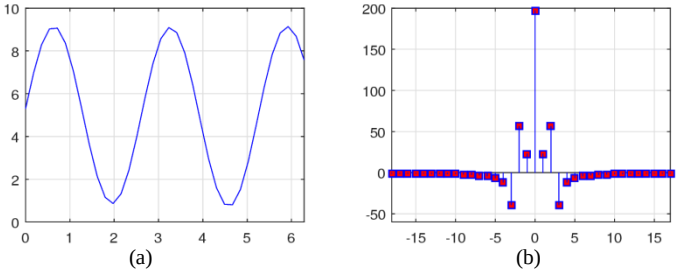

Figure 6. (a) The real signal and (b) the real part of the 36-point EDFT.

The imaginary part of the EDFF of the signal is shown in Fig. 7 in part (a), together with the imaginary part of the DFT of the signal in part (b). The semi-minor axis $b = 11.4103$; the range of the imaginary part of the transform in part (a) is b times larger than the imaginary part of the DFT.

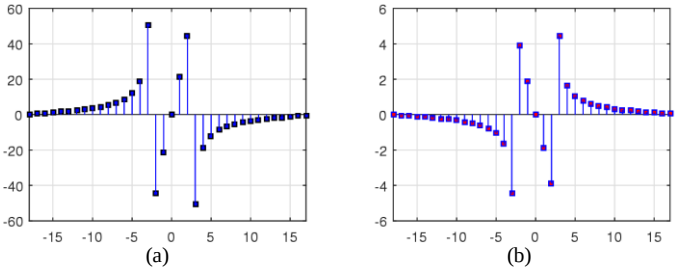

Figure 7. The imaginary part of (a) the 36-point EDFT and (b) the 36-point DFT.

 ISSN: 2454-4248
378 – 387

Figure 8 shows the magnitude $\sqrt{R_p^2 + I_p^2}$, $p = -18{:}\,17$, of the 36-point EDFT in part (a) and the magnitude of the 36-point DFT of the signal in part (b). One can note that the EDFT enhances the low-frequency components.

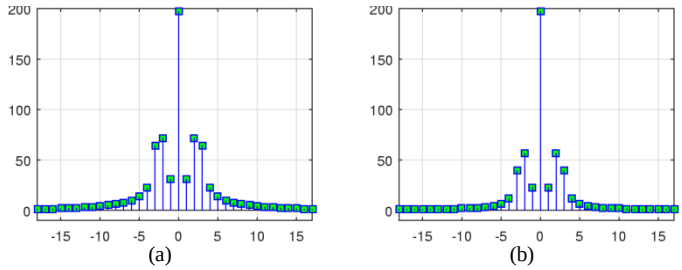

Figure 8. The magnitude (a) of the 36-point EDFT and (b) of the 36-point DFT.

When applying the 2-D EDFT to real images, the 1-D EDFTs with real inputs are used by rows and then, on the second stage of calculation, the 1-D EDFTs are used along the columns which represent complex inputs. To demonstrate the EDFT on the complex signal, we consider the complex signal $f(n) = x_r(n) + ix_i(n)$ of length 36, where the real part $x_r(n)$ is the signal

$$x_r(t) = 5 + 0.1\cos(2\omega_0 t) + 0.2\cos(5\omega_0 t) + 4\sin(6\omega_0 t),$$

with the frequency $\omega_0 = 2\pi/36$, and the imaginary part $x_i(n)$ is calculated from the signal

$$x_i(t) = 1 - 0.5\sin(6\omega_0 t) - 4;$$

both signals are sampled in the same time-interval $[0,2\pi]$. This complex signal is shown in Fig. 9.

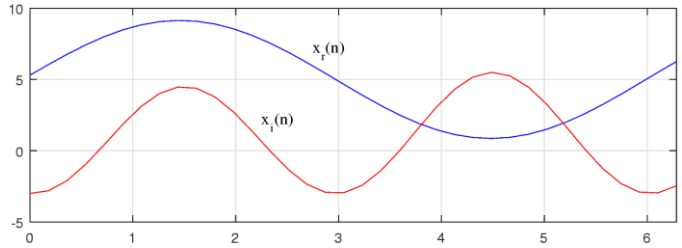

Figure 9. Two components of the complex signal of length 36.

Figure 10 shows the real and imaginary parts of the 36-point EDFT of the complex signal in parts (a) and (b), respectively.

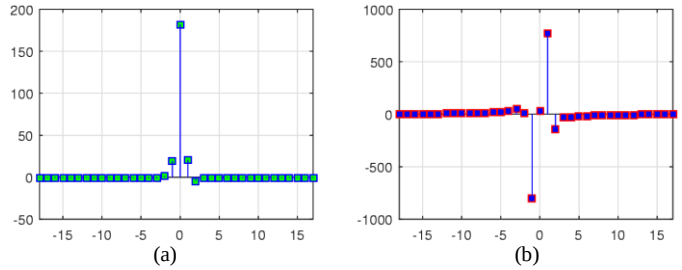

Figure 10. (a) The real part and (b) the imaginary part of the 36-point EDFT.

Figure 11 shows the magnitude of the 36-point EDFT in part (a). The magnitude of the 36-point DFT of this signal is shown in part (b), for comparison. One can notice that while preserving the value at frequency-point $p = 0$, the components of the EDFT at frequency-points $p = -1,1$, and 2 have larger magnitudes, when comparing with the DFT. The DC coefficient, i.e., the component F_0, is the same, 183.97.

Now we describe the proposed method of image processing in Eq. 16 for 1-D signals:

$$\boldsymbol{f} \to \boldsymbol{g} = \boldsymbol{M}_N\big(G(\phi_1)\big)\boldsymbol{f} \to \hat{\boldsymbol{f}} = \boldsymbol{M}_N(G^{-1}(\phi_2))\boldsymbol{g}, \qquad (18)$$

where ϕ_1 and ϕ_2 are two given angles. Here, $\boldsymbol{f}$ stands for the input signal $f(n) = x_r(n) + ix_i(n)$ and $\hat{\boldsymbol{f}}$ for the output signal $\hat{f}(n) = y_r(n) + iy_i(n)$.

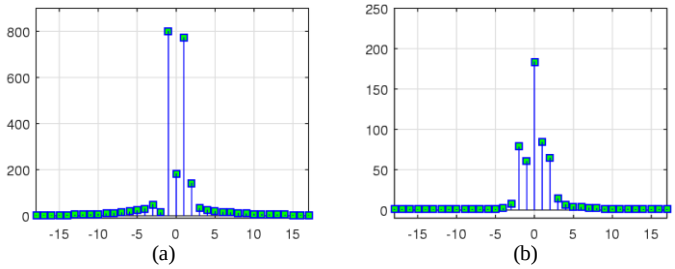

Figure 11. The magnitude (a) of the 36-point EDFT and (b) of the 36-point DFT.

We consider an example of processing a complex signal by the model described in Eq. 18. Figure 12 shows the original complex signal $\boldsymbol{f}$ in part (a) and the processed signal $\hat{\boldsymbol{f}}$ in part (b). In this case, the angles $\phi_1 = \varphi = 2\pi/36$ and $\phi_2 = \phi_1 + 0.1$.

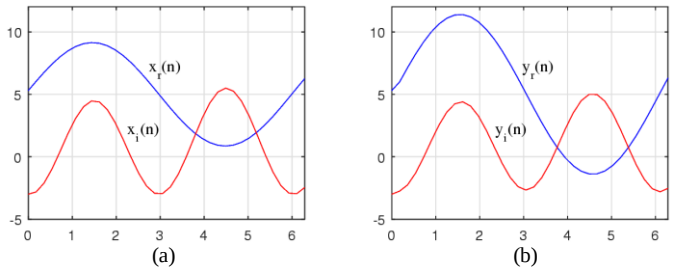

Figure 12. The complex signal (a) before and (b) after processing.

Also, we illustrate the $\phi_2 < \phi_1$ case, namely, when the angles $\phi_1 = \varphi = 2\pi/36$ and $\phi_2 = \phi_1 - 0.1$. Figure 13 shows the original signal $\boldsymbol{f}$ and processed signal $\hat{\boldsymbol{f}}$ in parts (a) and (b), respectively.

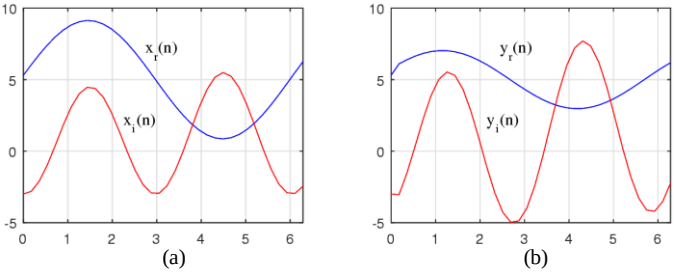

Figure 13. The complex signal (a) before and (b) after processing.

One can notice that in both considered cases the values of the first and last points of the signals are preserved. For other points, we can say the following. In the first case, when

 ISSN: 2454-4248
378 – 387

$\phi_2 > \phi_1$, the amplitude of the real part of the output signal is larger and the amplitude of the imaginary part is smaller than the input signal has. In the second case when $\phi_2 < \phi_1$, the amplitude of the imaginary part becomes larger and the amplitude of the real part of the signal is smaller than the original signal has. Thus, the angles ϕ_1 and ϕ_2 of two 1-D EDFTs that are used in the described signal processing are control parameters that allow to manipulate the real and imaginary parts of the transform.

A. *Analytical formula for processing images by two different 2-D EDFTs*

In the matrix $\boldsymbol{M}(G) = \boldsymbol{M}\big(G(\phi)\big)$, each (n,p)-th block is the 2×2 matrix $G^{np} = \cos(2\pi np/N)\, I + \sin(2\pi np/N)\, R(\phi)$. Therefore, if we denote by $\boldsymbol{C}$ the $N\times N$ matrix of cosine coefficients $\{\cos(2\pi np/N); n,p = 0{:}(N-1)\}$ and by $\boldsymbol{S}$ the $N\times N$ matrix of sine coefficients $\{\sin(2\pi np/N); n,p = 0{:}(N-1)\}$, the $2N\times 2N$ matrix $\boldsymbol{M}(G)$ can be written as

$$\boldsymbol{M}(G) = \boldsymbol{C}\otimes I + \boldsymbol{S}\otimes R(\phi). \tag{19}$$

Here, $\otimes$ denotes the tensor product of matrices. Thus, the N-point EDFT can be calculated by fast algorithms of the DFT.

It should be noted that the cosine and sine waves $c_{p_1}(n) = \cos(2\pi np_1/N)$ and $s_{p_2}(n) = \cos(2\pi np_2/N)$ are orthogonal functions. Here, $p_2 \neq p_1$ are integers in the interval $[0, N-1]$. In other words,

$$\sum_{n=0}^{N-1} c_{p_1}(n)\, c_{p_2}(n) = \sum_{n=0}^{N-1} s_{p_1}(n)\, s_{p_2}(n) = 0,$$

when $p_2 \neq p_1$ and

$$\sum_{n=0}^{N-1} c_{p_1}(n)\, s_{p_2}(n) = 0.$$

Therefore, the product of matrices $\boldsymbol{C}$ and $\boldsymbol{S}$ is zero, i.e., $\boldsymbol{CS} = \boldsymbol{SC} = \boldsymbol{0}$. The inverse matrix $\boldsymbol{M}(G)^{-1}$ can be written as

$$\boldsymbol{M}(G)^{-1} = \frac{1}{N}[\boldsymbol{C}\otimes I - \boldsymbol{S}\otimes R(\phi)]. \tag{20}$$

Indeed, the following calculations hold:

$$[\boldsymbol{C}\otimes I + \boldsymbol{S}\otimes R(\phi)][\boldsymbol{C}\otimes I - \boldsymbol{S}\otimes R(\phi)] = \boldsymbol{C}^2\otimes I - \\ -\boldsymbol{S}^2\otimes R(\phi) = \boldsymbol{C}^2\otimes I - \boldsymbol{S}^2\otimes R^2(\phi) = \boldsymbol{C}^2\otimes I + \boldsymbol{S}^2\otimes I = \\ (\boldsymbol{C}^2 + \boldsymbol{S}^2) = \boldsymbol{I}\otimes I = \boldsymbol{E}.$$

Here, I is the 2×2 identity matrix, $\boldsymbol{I}$ is the $N\times N$ identity matrix, and $\boldsymbol{E}$ is the $2N\times 2N$ identity matrix. In calculation of the inverse N-point EDFT, the rotation of data is accomplished in opposite direction, i.e., all angles of rotations change the signs, $\varphi_{np} \to -\varphi_{np}$, therefore $\boldsymbol{C}\to\boldsymbol{C}$ and $\boldsymbol{S}\to -\boldsymbol{S}$. Then, Eq. (17) leads to Eq. (18) with the normalized factor of N.

In the model of image processing in Eq. (16), the 1-D EDFTs with different second angles ϕ_1 and ϕ_2 are used for the direct and inverse 2-D EDFTs, respectively. The matrices of these 1-D EDFTs can be written as

$$\boldsymbol{M}(G) = \boldsymbol{M}\big(G(\phi_1)\big) = \boldsymbol{C}\otimes I + \boldsymbol{S}\otimes R(\phi_1), \tag{21}$$

$$\boldsymbol{M}(G)^{-1} = \boldsymbol{M}(G(\phi_2))^{-1} = \frac{1}{N}[\boldsymbol{C}\otimes I - \boldsymbol{S}\otimes R(\phi_2)]. \tag{22}$$

The same matrices are used in the 1-D version of this model described by Eq. (18). Therefore, the processing of the 1-D data in this model can be described by the transform with the matrix that is calculated as follows:

$$\boldsymbol{A}(\phi_1,\phi_2) = \frac{1}{N}\big[[\boldsymbol{C}\otimes I - \boldsymbol{S}\otimes R(\phi_2)]\big][\boldsymbol{C}\otimes I + \boldsymbol{S}\otimes R(\phi_1)] \\ = \frac{1}{N}[\boldsymbol{C}^2\otimes I - \boldsymbol{S}^2\otimes R(\phi_2)R(\phi_1)]. \tag{23}$$

Here, we mention that $R(\phi_2)R(\phi_1) \neq R(\phi_1)R(\phi_2)$.

VI. The Preliminary Experimental Results

In this section, a few examples of image enhancement are illustrated, by using the model given in Eq. 16. The enhancement of grayscale images is estimated by the quantitative measure of image enhancement that is known as the EME measure. This measure is defined as follows [25]-[27]. The image $f_{n,m}$ of size $N\times M$ is divided by small blocks, let say of size 7×7 each. The measure of the image after enhancement, $f_{n,m} \to \hat{f}_{n,m}$, is calculated by

$$EME\big(\hat{f}\big) = \frac{1}{k_1 k_2}\sum_{k=1}^{k_1}\sum_{l=1}^{k_2} 20\ln\frac{\max_{k,l}\big(\hat{f}\big)}{\min_{k,l}\big(\hat{f}\big)}. \tag{24}$$

Here, k_1 and k_2 are the numbers of blocks along two dimensions, i.e., $k_1 = \lfloor N/7\rfloor$ and $k_2 = \lfloor M/7\rfloor$ with the floor rounding. The operations $\max_{k,l}(\hat{f})$ and $\min_{k,l}(\hat{f})$ are the maximum and minimum of the image $\hat{f}_{n,m}$ inside the (k,l)th block, respectively.

As an example, Figure 14 shows the grayscale image of size 236×236 in part (a) and image enhanced by two 2-D EDFTs with parameters $\phi_1 = \varphi = 2\pi/236$ and $\phi_2 = \phi_1 + 0.0066$ in part (b). A very small change is done in the angle ϕ_1. The enhancement measure of the image is $EME(f) = 15.56$ and $EME\big(\hat{f}\big) = 20.31$, after processing. Thus, the image is enhanced by $\Delta EME = 20.31 - 15.56 = 4.75$.

(a) (b)

Figure 14. The grayscale image (a) before and (b) after enhancement by the 2-D EDFTs.

The image can also be processed by parts, for instance by parts of size 8×8, 16×16, or 32×32 each. As an example, we consider the "boat" image of size 512×512, that is shown in Fig. 15 in part (a). The image processed block-wise by two 2-D EDFTs with angles $\phi_1 = \pi/6$ and $\phi_2 = 1.75\phi_1$ is shown in part (b). The block size is 8×8, and the image enhancement

 ISSN: 2454-4248
378 – 387

measure of the original and processed images equals 10.9487 and 13.9737.

(a) (b)

Figure 15. (a) The original 'boat' image and (b) the image enhanced block-wise by the 2-D EDFTs .

Figure 16 shows the 512×512 image in part (a). The image processed by blocks of size 32×32 and two 2-D EDFTs with angles $\phi_1 = \pi/6$ and $\phi_2 = 1.75\phi_1$ is shown in part (b). The image enhancement measure of the original equals 15.63 and for the processed image is 23.79.

(a) (b)

Figure 16. The grayscale image (a) before and (b) after enhancement block-wise by the 2-D EDFTs.

Figure 17 shows the "Goldhill" image of size 512×512 in part (a). The image enhancement by two 2-D EDFTs with the same angles is shown in parts (b) and (c), when blocks of size 8×8 and 16×16 were used, respectively. For the original image, the measure EME is 10.14 and, for enhanced images in parts (b) and (c), the measure equals 16.69 and 17.36, respectively.

(a) (b) (c)

Figure 17. (a) The grayscale image and (b) image enhancement by 8×8 blocks and (c) by 16×16 blocks.

A. Color Image Processing

When processing a color image, for instance in the RGB color model, the red, green, and blue components of the image $f = \{f_R, f_G, f_B\}$ as grayscale images can be processed separately and the EME measure can be calculated for each color. However, the color enhancement measure known as EMEC can also be used [28,29,31,32]. This measure is similar to EME and is calculated by

$$EMEC(\hat{f}) = \frac{1}{k_1 k_2} \sum_{k=1}^{k_1} \sum_{l=1}^{k_2} 20\log_{10} \left[\frac{\max_{k,l}(\hat{f}_R, \hat{f}_G, \hat{f}_B)}{\min_{k,l}(\hat{f}_R, \hat{f}_G, \hat{f}_B)} \right]. \quad (25)$$

Here, the maximum of the image in the (k,l)-th block is calculated component-wise as $\max\left[(\hat{f}_R)_{n,m}, (\hat{f}_G)_{n,m}, (\hat{f}_B)_{n,m}\right]$. The minimum in the block is calculated similarly. To avoid zeros in the denominator in Eq. (25), the constant 1 can be added to each color component of the image.

Figure 18 shows the result of image enhancement, when all three color components of the image are processed by the same values of parameters ϕ_1 and ϕ_2, that are used for the image in Fig. 14. The original color image is shown in Fig. 18 in part (a) and the enhanced image in part (b). The enhancement measure for the original color image is $EMEC(f) = 32.29$ and for the enhanced image is $EMEC(\hat{f})$ =37.25. Thus, the color image is enhanced by $\Delta EMEC = 37.25 - 32.29 = 4.96$.

(a) (b)

Figure 18. (a) The original color image and (b) the image enhanced channel-wise by two 2-D EDFTs with angles $\phi_1 = 2\pi/236$ and $\phi_2 = \phi_1 + 0.0066$.

Figure 16 shows all color components of the image before and after enhancement. One can notice that all colors were enhanced.

 ISSN: 2454-4248
378 – 387

(a) (b)

Figure 19. The red, green, and blue components of the color image (a) before and (b) after processing.

Figure 17 shows another color image of size 428×428 in part (a) and its enhancement in part (b). In this image enhancement, for direct 2-D EDFT the 1-D EDFT is used with the matrix $\boldsymbol{M}(G(\pi/6))$, and for the inverse 2-D EDFT the 1-D EDFT is used with matrix $\boldsymbol{M}(G(\pi/4))$.

(a) (b)

Figure 17. (a) The original color image and (b) the image enhanced channel-wise by the 2-D EDFTs with angles $\phi_1 = \pi/6$ and $\phi_2 = \pi/4$.

The above examples show that, by only manipulating with the second angles ϕ_1 and ϕ_2, grayscale and color images can be enhanced in the proposed model. However, a criterion for automatic selection of these angles for image enhancement with desired outcomes is not clear yet. This problem for color images is complex since each color component can be processed with different 2-D EDFTs.

The elliptic DFTs represent a class of transforms that do not include the traditional DFT that allows rotating input data only around circles. The rotation of data in the elliptic DFTs is accomplished around ellipses not circles. We believe that new methods with these transforms will be found and effectively used in imaging.

REFERENCES

[1] D. Wang and A.H. Vagnucci, “Digital image enhancement,” Computer Vision, Graphics, Image Processing, vol. 24, pp. 363-381, 1981.

[2] P. Zamperoni, “Image enhancement,” Advanced in Image and Electron Physics, vol. 92, pp. 1–77, 1995.

[3] A. Laine, J. Fan, W. Yang, “Wavelets for contrast enhancement of mammography,” IEEE Eng. Med. Biol, vol. 14, pp. 536-550, 1995.

[4] S.S. Agaian, K. Panetta, A.M. Grigoryan, “Transform-based image enhancement algorithms,” IEEE Trans. on Image Processing, vol. 10, no. 3, pp. 367–382, 2001.

[5] A.M. Grigoryan, S.S. Agaian, “Transform-based image enhancement algorithms with performance measure,” Advances in Imaging and Electron Physics, Academic Press, vol. 130, pp. 165–242, 2004.

[6] J. Xia, K.A. Panetta, S. Agaian, “Color image enhancement algorithm based on DCT transforms,” Proc. Man and Cybernetics, SMC 2011. IEEE International Conference, Alaska, pp. 1496-1501, 2011.

[7] K. Panetta, J. Xia, S. Agaian, “Color image enhancement based on the discrete cosine transform coefficient histogram,” Journal of Electronic Imaging, Apr-Jun 2012, vol. 21, no. 2, pp. 021112-1, 021112-17, 2012.

[8] A.M. Grigoryan, M.M. Grigoryan, “Discrete signal induced unitary transforms,” 577-827, pp. 26-31, American Conference on Applied Mathematics, WSEAS 2008, Cambridge, March 2008.

[9] F.T. Arslan, A.M. Grigoryan, "Enhancement of medical images by the paired transform,” Proc. of the 14th IEEE International Conference on Image Processing, vol. 1, pp. 537-540, San Antonio, Texas, September 16-19, 2007

[10] K. Naghdali, R. Ranjith, A. Grigoryan, “Fast signal-induced transforms in image enhancement,” Proc. Systems, Man and Cybernetics, SMC 2009. IEEE Int. Conference on, pp. 565-570, Oct 2009.

[11] J.H. McClellan, “Artifacts in alpha-rooting of images,” Proc. IEEE Int. Conf. Acoustics, Speech, and Signal Processing, pp. 449-452, Apr. 1980.

[12] A.M. Grigoryan, S.S. Agaian, Multidimensional Discrete Unitary Transforms: Representation, Partitioning and Algorithms. Dekker, New York, 2003.

[13] F.T. Arslan, A.M. Grigoryan, “Fast splitting alpha-rooting method of image enhancement: Tensor representation,” IEEE Trans. on Image Processing, vol. 15, no. 11, pp. 3375–3384, Nov. 2006.

[14] J.W. Cooley, J.W. Tukey, “An algorithm the machine computation of complex Fourier series,” Math. Comput. vol. 9, no. 2, pp. 297–301, 1965.

[15] D.F. Elliot, K.R. Rao, Fast Transforms-Algorithms, Analyzes, and Applications. Academic Press, San Diego, 1982.

[16] R.E. Blahut, Fast Algorithms for Digital Signal Processing. Addison-Wesley, Reading, 1985.

[17] P. Duhamel, M. Vetterli, “Fast Fourier transforms: a tutorial review and state of the art,” Signal Process, vol. 19, pp. 259–299, 1990.

[18] A.M. Grigoryan, S.S. Agaian, “Split manageable efficient algorithm for Fourier and Hadamard transforms,” IEEE Trans. on Signal Processing, vol. 48, no. 1, pp. 172-183, Jan. 2000.

[19] A.M. Grigoryan, “2-D and 1-D multi-paired transforms: Frequency-time type wavelets,” IEEE Trans. on Signal Processing, vol. 49, no. 2, pp. 344-353, Feb. 2001.

[20] A.M. Grigoryan, V.S. Bhamidipati, “Method of flow graph simplification for the 16-point discrete Fourier transform,” IEEE Trans. Signal Process, vol. 53, no. 1, pp. 384–389, 2005.

[21] A.M. Grigoryan, M.M., Grigoryan, Brief Notes in Advanced DSP: Fourier Analysis with MATLAB, Taylor & Francis/CRC Press, London/Boca Raton, 2009.

[22] A.M. Grigoryan, M.M. Grigoryan, “Discrete integer Fourier transform in real space: Elliptic Fourier transform,” [7245A-1], International Conference: Electronic Imaging, Science and Technology, IS&T/SPIE 21st Annual Symposium, San Diego, CA, 18-22 January, 2009.

[23] A.M. Grigoryan, “Elliptic discrete Fourier transforms of Type II,” Proc. 2009 IEEE International Conference on Systems, Man, and Cybernetics, pp. 954–959, San Antonio, Texas, USA, 2009.

 ISSN: 2454-4248
378 – 387

[24] A.M. Grigoryan, "Two classes of elliptic discrete Fourier transforms: Properties and examples," Journal of Mathematical Imaging and Vision (0235), vol. 39, pp. 210-229, January 2011.

[25] S.S. Agaian, K. Panetta, A.M. Grigoryan, "A new measure of image enhancement," Proc. IASTED Int. Conf. Signal Processing & Communication, Marbella, Spain, pp. 19–22, 2000.

[26] E.Wharton, S. Agaian, K. Panetta, "Comparative study of logarithmic enhancement algorithms with performance measure," Proc. SPIE 6064, Image Processing: Algorithms and Systems, Neural Networks, and Machine Learning, 606412, February 2006.

[27] A.M. Grigoryan, S.S. Agaian, "Adapted retinex algorithm with complexity optimization for mobile phone medical image enhancement," chapter 5, pp. 119-151. In Electronic Imaging Applications in Mobile Healthcare, (J. Tang, S.S. Agaian, and J. Tan, Eds., SPIE Press, Bellingham, Washington, February 2016.

[28] A.M. Grigoryan, S.S. Agaian, "Color enhancement and correction for camera cell phone medical images using quaternion tools," Chapter 4, pp. 77–117. In book: Electronic Imaging Applications in Mobile Healthcare, (J. Tang, S.S. Agaian, and J. Tan, Eds.,) SPIE Press, Bellingham, Washington, 2016.

[29] A.M. Grigoryan, S.S. Agaian, "Image processing contrast enhancement," 22p, Wiley Encyclopedia of Electrical and Electronics Engineering, May 2017 (doi: 10.1002/047134608X.W5525.pub2)

[30] A.M. Grigoryan, J. Jenkinson, S.S. Agaian, "Quaternion Fourier transform based alpha-rooting method for color image measurement and enhancement," SIGPRO-D-14-01083R1, Signal Processing, vol. 109, pp. 269–289, April 2015, (doi:10.1016/j.sigpro.2014.11.019).

[31] A.M. Grigoryan, S.S. Agaian, Practical Quaternion Imaging with MATLAB, SPIE Press, March 2018.

[32] A.M. Grigoryan, S.S. Agaian, "Alpha-rooting method of gray-scale image enhancement in the quaternion frequency domain," Proc. IS&T International Symposium, Electronic Imaging: Algorithms and Systems XV, Jan.-Feb., Burlingame, CA, 2017.